2000

Surface Effects on the Dynamics of Liquid Crystalline Thin Films Confined in Nanoscale Cavities

Alison Noble
Messiah University, anoble@messiah.edu

Ralph G. Nuzzo

Renée M. Blanchard

Surface Effects on the Dynamics of Liquid Crystalline Thin Films Confined in Nanoscale Cavities

Alison R. Noble-Luginbuhl

Renée M. Blanchard

Ralph G. Nuzzo

Abstract

The dynamics of 4-*n*-pentyl-4‘-cyanobiphenyl (5CB) nematic liquid crystalline thin films have been studied in real time using step-scan Fourier transform infrared spectroscopy (FTIR). In these studies, the liquid crystal was confined in a nanocavity defined and bounded by an interdigitated gold electrode array. The gold microstructures were microfabricated on a zinc selenide (IR-transparent) window. The 5CB interactions with the ZnSe substrate result in surface-induced ordering of the ultrathin layers (on the order of 40 nm). As the films increase in thickness, the nanoscale organization induced by the surface layer becomes a less significant contributor to the overall bulk structure of the sample. Time-resolved FTIR studies have enabled the measurement of rate constants for the orientation and relaxation of the thin films under an applied electric field as a direct function of confinement dimensions. Cell thicknesses ranging from 40 to 300 nm were studied. The measured rate behaviors demonstrate the strong effects of the interactions occurring between the surfaces of the ZnSe crystals and the 5CB on the dynamics of the liquid crystalline assembly. Time-resolved studies reveal kinetically inhomogeneous line shapes for thicker films while ultrathin films maintain kinetically homogeneous peaks, suggesting the development of liquid crystalline domains or other inhomogeneities over this length scale in the transition from the surface layer to bulk.

Introduction

Developing an improved understanding of the molecular-level sensitivities of thin-film dynamics to interactions occurring at surfaces and interfaces is a central need for the development of a wide range of materials technologies. Representative examples of areas in which such behaviors of an organic thin film figure prominently include coatings inhibiting corrosion,[1] chemical separations involving transport and adsorbate binding in thin-film boundary layers,[2,3] and the complex functioning of biological membranes (e.g., in recognition signaling and active transport).[4] This report concerns itself with the electrooptical properties and dynamics of nanoscale thin films of liquid crystals, materials that are central to the operation of liquid crystal (LC) displays.[5] It is now well appreciated that a detailed understanding of the dynamics of liquid crystalline materials, and their sensitivity to the strong surface binding (so-called anchoring) interactions that occur at the cell boundaries, is fundamental to developing improved devices.[5]
A number of excellent studies have appeared in which the nature and consequences of these interactions have been examined.[6-10] The molecular design of the surface binding interactions through the use of self-assembled monolayers (SAMs) has proven to be an

extremely useful way to manipulate and tailor the LC anchoring interactions.[11-16] In this study, we concern ourselves with the less well studied and still poorly understood matter of the dynamics of a LC thin-film boundary layer in the strong binding limit. This work employed an IR cell of unique design[17] to examine the electrodynamic responses of extremely thin liquid crystalline films to perturbations imposed by an electric field. The present report demonstrates and characterizes the profound effects of surface binding interactions on both the orientation and relaxation dynamics of these prototypical nanoscale organic thin films as well as the length scales over which a transition to bulklike properties occurs.

Experimental Methods

The fabrication method used to construct an interdigitated array electrode (IDA) thin-film cell supported on a ZnSe IR window is described elsewhere.[17] In this study, IDAs with gold electrodes 40 and 300 nm thick were fabricated. To minimize diffraction effects, we used a design based on 15 μm gold bands separated by 15 μm spaces. Two 1 μL drops of 4-*n*-pentyl-4‘-cyanobiphenyl (5CB; BDH Chemical, England) were placed onto the IDA fingers to ensure that all the spaces between the fingers were filled. An unpatterned ZnSe window was then placed on top of the patterned window and the cell compressed using metal weights to squeeze out the excess 5CB and bring the gold fingers into contact with the second ZnSe window. The nanocavities are formed by the gold IDA bands which serve as a shim for the ZnSe windows. It is likely that some 5CB is entrained between the gold bands and the ZnSe crystal. This quantity appears to be very small, perhaps of the order of a monolayer or so and, thus, is not of consequence for the homogeneity of the electric field intensities experienced by molecules residing between the electrode bands. The cell was fabricated and assembled in a clean room to prevent airborne particulates (which can exceed several microns in size) from being caught in the assembly and thus controlling the thickness of the confined layer. After the cell was assembled, the top window was gently sheared back and forth along the direction of the interdigitated bands. The cell was then placed in a stainless steel sample holder and the areas of the sample surrounding the IDA were masked to ensure IR response only from those areas patterned with electrodes (using an open aperture, we probed the entire masked area: a rectangle measuring 1.0 × 0.30 cm).

After filling the cell with 5CB, a dc potential between 10 and 15 V was repeatedly applied across the IDA. This perturbation eliminated hysteresis induced by the initial contact and spread of 5CB across the ZnSe and allowed the molecules to settle into a reproducible state (sans electric field).

All infrared measurements were taken with a Bio-Rad (Cambridge, MA) FTS 6000 spectrometer equipped with a KBr beam splitter and high-temperature ceramic source. A rotatable KRS-5 Au wire-grid polarizer was placed in the beam path to select IR radiation polarized in directions parallel and perpendicular to the IDA bands. All scans were taken using Bio-Rad Win-IR Pro software designed for data acquisition with the FTS 6000 spectrometer. The collected interferograms were single-sided (asymmetric) and a triangular apodization algorithm was used to weight the interferogram. For both rapid-scan and step-scan experiments, a nitrogen-cooled mercury cadmium telluride (MCT) detector (Bio-Rad) equipped with a dc-coupled preamplifier was used.

Two distinct spectroscopic experiments are reported here: those involving (1) static and (2) dynamic electrical polarization. Rapid-scan experiments used to probe the system under static voltage conditions were carried out with an optical modulation of 20 kHz, a 5 kHz low-pass filter, and a spectral resolution of 4 cm^{-1}. For each spectrum, 1024 scans were collected and averaged. To apply a voltage across the cell, a dc power supply with an output range of 0−15 V was used. Due to the difference in refractive index between ZnSe, 5CB, and air, it was difficult to obtain background spectra without encountering interference fringes. Because of this problem, a more experimentally efficient reference scheme was adopted for most of the experiments described below. In these studies, a single-beam spectrum of the 5CB-filled cell at 0 V was used as the background and the field response data were computed and presented as difference (rather than absolute) spectra.

The time-resolved data were acquired at a scan rate of 5 Hz with time resolution set at 375 μs for a set of 16 coadded scans. The spectral resolution of the scans was 4 cm^{-1} and the spectral range was limited to 0−3950 cm^{-1} using an optical long-pass filter (Bio-Rad) and an undersampling ratio of 4. Background scans were collected with the same setup, but with the IDA disconnected from the voltage source.

Dynamic electrical polarization experiments were conducted using a programmed modulation. A Wavetek function generator applying a square wave pulse of 12.6 V across the IDA supplied the cyclic perturbation during the step-scan experiment. The width of the pulse was 50 ms (with a rise time of <5 μs) and was applied following every mirror step after a 25 ms settling time. This program of the applied potential allowed a complete relaxation of the prepared cell from the perturbed state.

Results

The liquid crystalline material studied here is the nematic phase of 5CB,[18] the structure of which is shown in Figure 1. When the molecule is exposed to an electric field of sufficient magnitude, its molecular axis reorients along the direction of the applied field. The threshold voltage required to initiate reorientation of the molecule is called the critical voltage. This electric field-induced orientation of a liquid crystal (Freedericksz transition)[19] occurs because of the positive dielectric anisotropy of the 5CB structure.[20] This voltage is not sufficiently large so as to eliminate the stronger dimerization of the 5CB dipoles in the nematic domains.

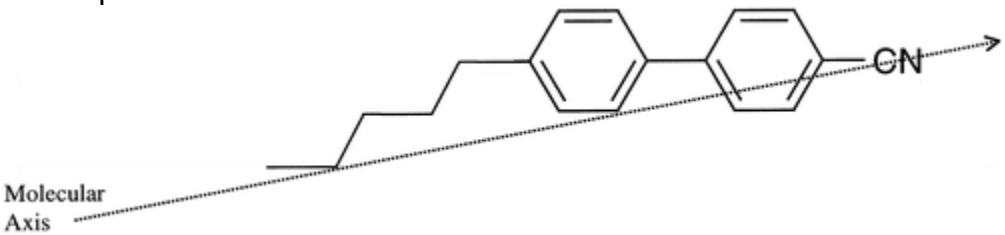

Figure 1 Structural diagram of 4-*n*-pentyl-4‘-cyanobiphenyl (5CB). The vector overlaying the structure of 5CB indicates the molecular axis used to define the orientation of the molecule.

Previous studies of organic liquid crystals using FTIR spectroscopy typically sandwich bulk samples of the material between two electrodes that are transparent in the infrared region (e.g., germainium).[10,21,22] When this sandwich geometry is used, the IR beam is incident in a direction parallel to that of the applied electric field (Figure 2) and thus the liquid crystal (5CB has a positive dielectric anisotropy) orients along the same direction as the propagation of the incident IR beam. Additionally, the substrate materials are limited to conductive materials that are also transparent in the frequency range of interest or nonconductive materials that can be coated with a transparent conductive film. Fewer reports appear to have adopted a cell design based on band electrodes.[23,24] A notable exception is the early report of Soref,[23] which describes the construction of a light valve based on a related (albeit differing) cell design.

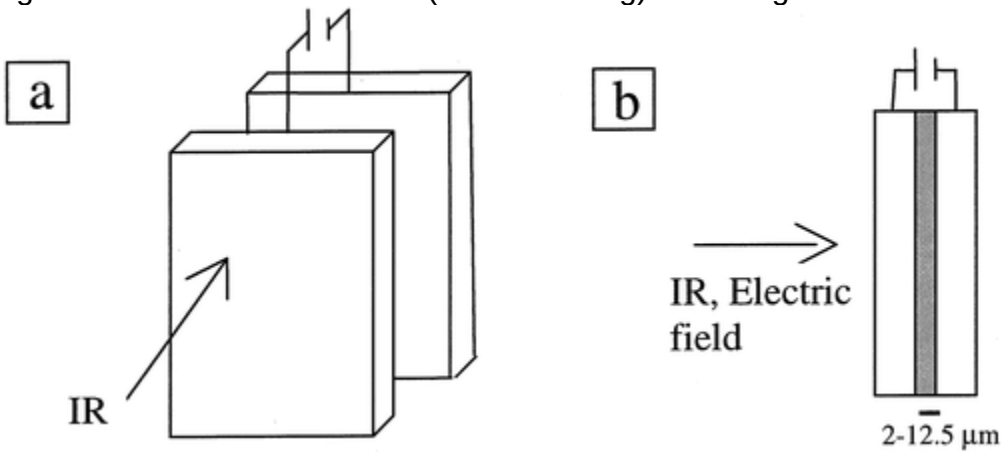

Figure 2 Configuration of IR cells typically used for confining liquid crystalline films (sandwich geometry): (a) expanded view and (b) cross-sectional view. The spacing between conductive windows is usually on the order of 2−12.5 μm.

An optical cell design employing an interdigitated array electrode[25,26] provides a unique sampling geometry for the time domain experiments of interest here and enables the confinement of extremely thin samples for study with infrared spectroscopy. The IDA-based design used in this study is shown in Figure 3a. An IDA consists of many parallel bands of electrodes each separated by an insulating gap. As shown in the figure, the electrode bands are connected alternately to create an array of electrode pairs. Fabrication of an IDA directly onto a ZnSe substrate provides the basis for the cell in which a thin film is confined in the gap between electrode bands by a second IR window placed directly on top of the IDA (Figure 3b). The thickness of the film can be varied continuously by changing the height of the IDA, provided that dust particles are excluded rigorously. We found that the fabrication and assembly had to be carried out in at least a class 100 clean room to meet the needs of this later requirement. In these transmission experiments, the plane of the IDA was oriented normal to the incident IR beam. The electric field is applied in the plane of the substrate and thus perpendicular to the direction of IR propagation. In this sampling geometry, the orientation of liquid crystals occurs along a direction transverse to the beam propagation and thus it is possible to observe changes in the optical anisotropy with a wide range of optical polarization vectors.

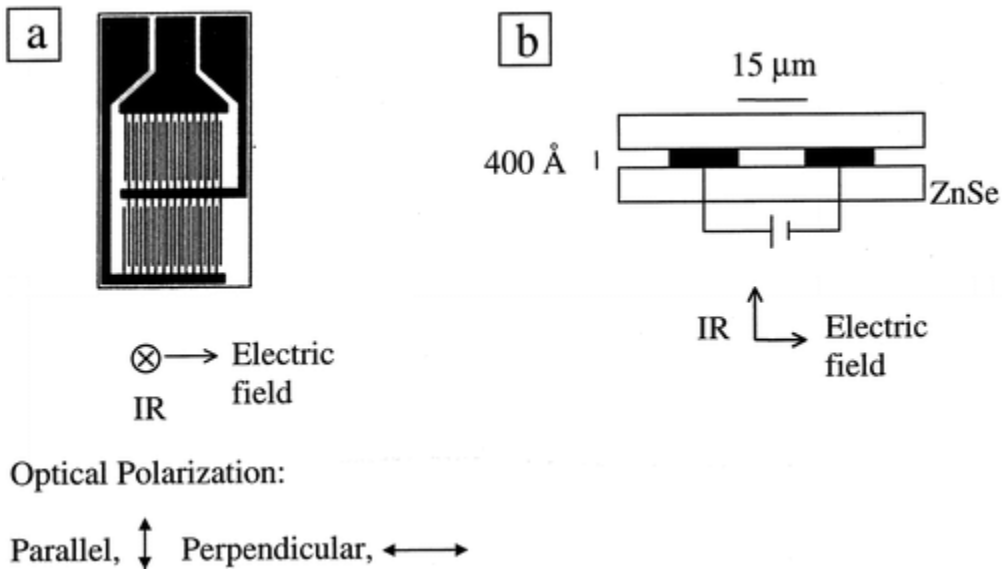

Figure 3 (a) Top view of an interdigitated electrode array (IDA) with optical polarization defined relative to the electrode fingers. (b) Cross section of thin-layer confinement cell with bands 15 µm wide and 15 µm from neighboring bands. The height of the IDA defines the thickness of the thin film. Shown here is the thinnest cell, 40 nm thick.

Previous studies have shown that the surface-induced orientation of a liquid crystal can have long-range effects on the bulk order.[12] In this study, we investigated the energetics and dynamics of the electric field-induced orientation of liquid crystalline films at two limiting thicknesses, 40 and 300 nm, to elucidate the nature of the changes that occur as the sample dimensions are varied from a thin- to thick-film limit. The IDA pitch and size (1 and 15 µm) allow for excellent throughput and provide a large in-plane confinement dimension. The optical design used here was deliberately selected to avoid diffraction effects and to minimize the contributions that result from the boundary layer optical effects due to the Au bands. (We will describe the purposeful exploitation of these latter two complex effects in future publications). The latter optical boundary layer effects (which have a node at the gold surface in the data taken with optical polarization parallel to the gold electrodes)[27] are identical for the varying Au electrode thicknesses studied. We use these gold bands as a variable shim to provide a flexible and easily adjusted transverse confinement dimension. The limiting thickness followed in this study (40 nm) corresponds to a layer that is only ~25 times larger than the long axis dimension of the 5CB molecule.

We use rapid-scan FTIR spectroscopy to determine the net anisotropy of the liquid crystalline medium both before and after the electric field is applied and step-scan FTIR[28-30] to study the dynamics of the orientation and relaxation processes of the confined samples. The latter time-domain measurements reveal important differences in the energetics of surface-dominated and more bulklike samples of the nematic liquid crystal. We describe the results obtained from each of these types of measurements in turn.

The Vibrational Spectrum of 5CB. A representative infrared difference spectrum of a thin film of 5CB (40 nm thick) is presented in Figure 4. Assignments for prominent

vibrational bands, along with estimates of their transition moment directions relative to the molecular coordinates as defined by the long axis vector[9,22,31] (Figure 1), are given in Table 1. For this spectrum, the cell was held at 15 V and the ratio of the single-beam spectrum was determined against a single-beam background spectrum measured with the cell held at 0 V. For the spectrum shown, the incident light was polarized perpendicular to the direction of the IDA fingers (and thus parallel to the applied electric field). In this paper, the IR polarization direction is defined with respect to the IDA fingers: a perpendicular orientation indicates that the IR radiation is polarized perpendicular to the electrode fingers (and therefore parallel with the applied electric field); a parallel orientation indicates that the radiation is polarized parallel to the IDA bands (see Figure 3a).

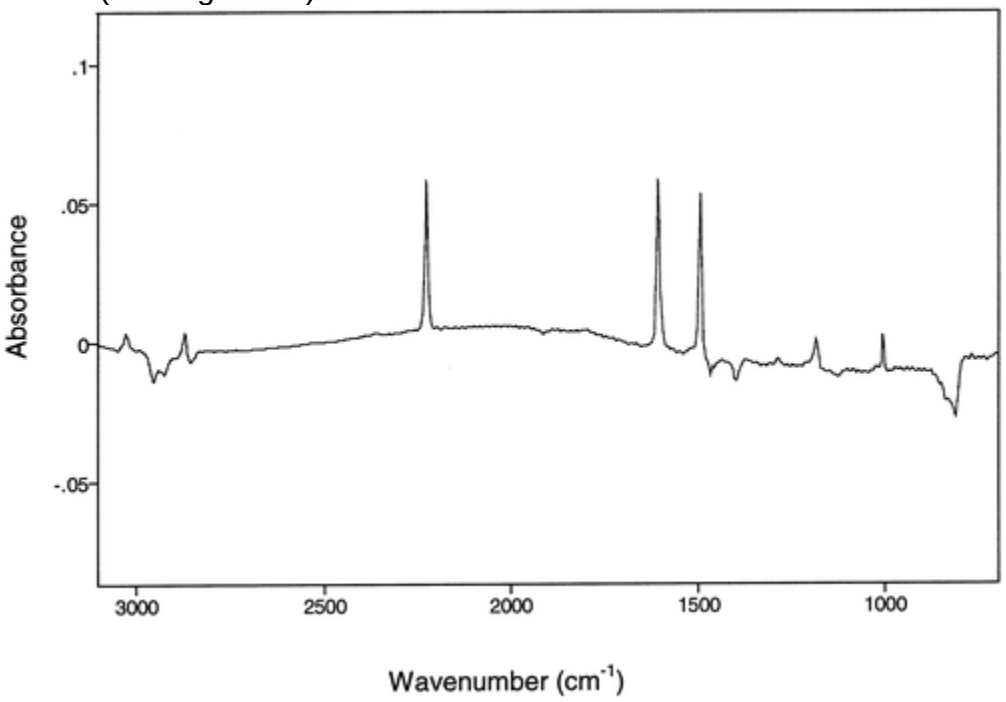

Figure 4 Infrared difference spectrum of 5CB taken with light polarized perpendicular to the IDA bands. The spectrum is the ratio of the 5CB-filled 40 nm cell held at 15 V to the same cell held at 0 V. Positive peaks show modes that have oriented perpendicularly to the IDA bands while negative peaks represent vibrational modes that have reoriented parallel to the IDA bands upon application of the electric field.

Table 1. Vibrational Mode Assignments for 5CB and the Transition Moment Direction Angle Relative to Molecular Axis Shown in Figure 1

wavenumber (cm^{-1})			
lit.[a]	obs	mode assignment	β^b (deg)
3025	3025	phenyl C−H stretch	
2957	2957	methyl degenerate antisymmetric C−H stretch	
2926	2930	methylene antisymmetric C−H stretch	58.8

2870	2872	methyl symmetric C−H stretch	
2857	2857	methylene symmetric C−H stretch	59.2
2226	2226	C:N stretch	20.0
1606	1606	phenyl C−C stretch	16.1
1494	1494	phenyl C−C stretch	15.5
1460	1466	C−H deformation of pentyl chain	
1397	1398	C−H deformation of pentyl chain	
1185	1185	phenyl C−H in-plane deformation	
1006	1006	phenyl C−H in-plane deformation, breathing	
818	814	phenyl C−H out-of-plane deformation	90

[a] References 9 and 22.[b] The angle between the transition moment direction and the molecular axis of the molecule.[31]

Vibrational modes absorb light that is polarized parallel to the transition moment direction.[32] Since we know the transition moment directions of the prominent vibrational bands (shown in Table 1) with respect to the molecular axis, it is possible to monitor changes in the orientation of the 5CB molecule under an applied electric field using polarized IR light. In difference spectra, the changes in a band's intensity is a direct measure of the net change in the anisotropy of the LC medium; since both positive and negative bands are possible, both a net gain or a net loss in orientation of a specific transition dipole moment along the direction of the polarization used can be monitored. The spectrum shown in Figure 4, for example, exhibits both positive and negative intensity bands (e.g., the ν_{CN} stretch at 2226 cm^{-1} and the C−H out-of-plane deformation at 814 cm^{-1}) as would be expected for the normal modes described in Table 1. Derivative-like line shapes are also seen in this spectrum; these arise from either peak shifts in a fundamental mode (an effect of lesser importance here) or the overlap of two modes with different transition moment directions (as is most evident in the C−H stretching region).

In this way, we are able to monitor the orientational changes of thin films of liquid crystal under an applied field as well as deduce important information about the net anisotropy of the liquid crystal prior to orientation. With regard to the latter point, the data shown in Figure 4 implicitly establishes that a significant anisotropy exists in this 5CB film. It is to this aspect that we now turn our attention.

Electric Field-Dependent Organization of 5CB. Our first experiments elucidated the net orientations of the 5CB molecules in the 40 and 300 nm films as a function of applied potential. Starting with a voltage of zero and increasing by 1 V increments up to 15 V, single-beam spectra of the cell were acquired and then the ratio to the zero voltage reference scan taken. The resulting set of difference spectra show that, via a highly anisotropic motion, the long axes of the 5CB molecules rotate progressively to a direction parallel with the applied field. The upper panel of Figure 5a presents the difference spectra for the CN stretching mode (centered at 2226 cm^{-1}) for the 40 nm film at successive voltage steps recorded with the incident light polarized perpendicular to the IDA fingers. The CN stretch has a large vector component along the long axis of the

molecule; thus, as it orients along the lines of the applied field, the CN peak intensities measured in this polarization increase. An analogous set of scans was collected using light polarized parallel to the IDA fingers (Figure 5a, lower panel). As is strikingly evident, the applied potential has little effect on the difference band intensities seen using this polarization (the spectra are essentially a baseline). A quantitative analysis of these data is given in Figure 6a, which plots the integrated absolute peak area of the ν_{CN} stretching mode versus the applied voltage for both $I_{\perp}$ and $I_{\parallel}$ spectra. These results suggest that the field-induced reorganization of the liquid crystal molecules in the 40 nm film was highly coherent throughout the sample, involving (at a minimum) components with orientations lying along a vector perpendicular to the surfaces of the ZnSe cell windows. Since the intensity increases in the $I_{\perp}$ direction, but does not decrease commensurately in the $I_{\parallel}$ orientation, the simplest analysis would suggest that the molecules in the 40 nm thin film project only weakly (if at all) onto the latter direction. In other words, there is a nearly homogeneous alignment of the 5CB along the transverse cell direction in the absence of an applied electric field. However, spectra taken at 0 V, when computed against an empty cell background spectrum (given in the Supporting Information), demonstrate unequivocally that the orientation of the 5CB long axis does in fact have projections along both the $I_{\parallel}$ and $I_{\perp}$ directions. Taken together, the data appear to suggest that the initial state has a net anisotropy along the transverse cell direction, but where the molecules are aligned with an azimuthally averaged orientation of tilts (Figure 7). The 15 μm spacing of the gold electrode fingers is not a sufficient perturbation to induce a net anisotropy of the tilt direction in this plane. This aligned state is a thermodynamically driven effect as revealed by the fact that the field-induced alignment relaxes completely to this same initial state. It is also interesting to note that the data clearly demonstrate a very strong anisotropy in the field-induced molecular motions. As shown in Figure 5a, the intensity gained in the $I_{\perp}$ direction must come from a reorientation of the 5CB transition moments moving out of the transverse cell direction. Since the average molecular orientation of 5CB at 0 V involves an azimuthally averaged orientation of the tilts, the field-induced motions cannot effect all parts of this ensemble equally. If this were not the case, then effects should be seen in the $I_{\parallel}$ direction. Figure 5a shows unambiguously that there is little or no change in the tilt anisotropies pointing along this direction in the 40 nm cell. A pictoral discription of the initial and field-induced orientations is shown in Figure 7.

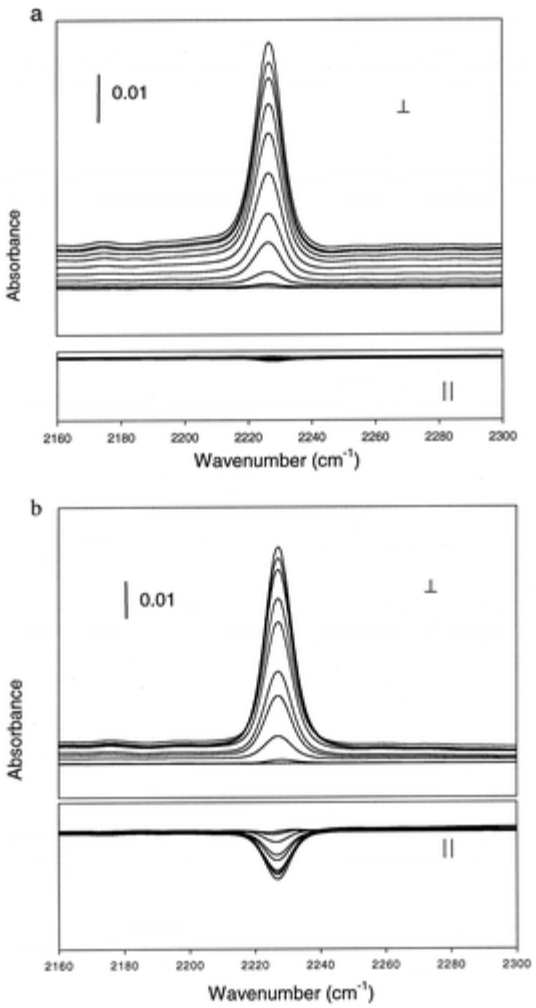

Figure 5 Difference peaks of the CN stretch for both parallel and perpendicular polarization as voltage is increased in increments from 1 to 15 V. Zero volts is used as the reference spectrum. (a) The 40 nm IR cell. The peaks with greatest intensity occur at the highest applied voltage (15 V) due to increased anisotropy induced by the applied field. No change is seen in the parallel polarization. (b) The 300 nm film of liquid crystal. Like the 40 nm film, the intensity in the perpendicular direction increases with increased voltage. However, in this thicker film, the intensity decreases when probed with light polarized parallel to the IDA fingers.

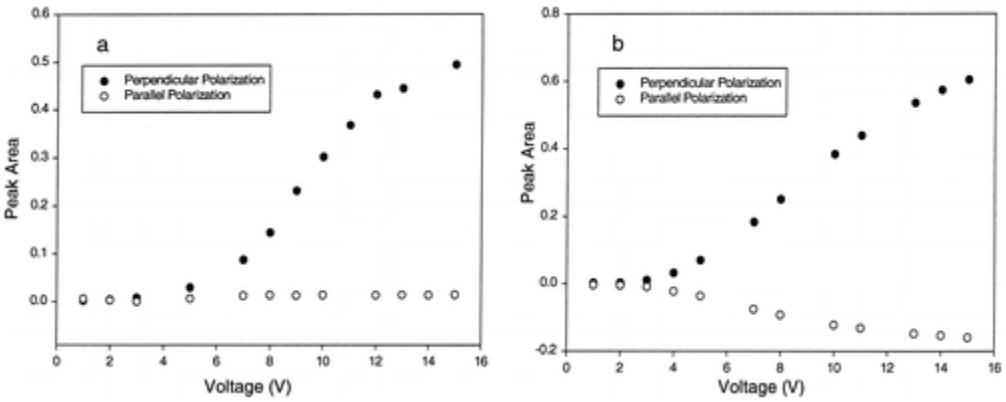

Figure 6 Peak area versus applied voltage for the CN stretch at 2226 cm^{-1}: (a) 40 and (b) 300 nm film.

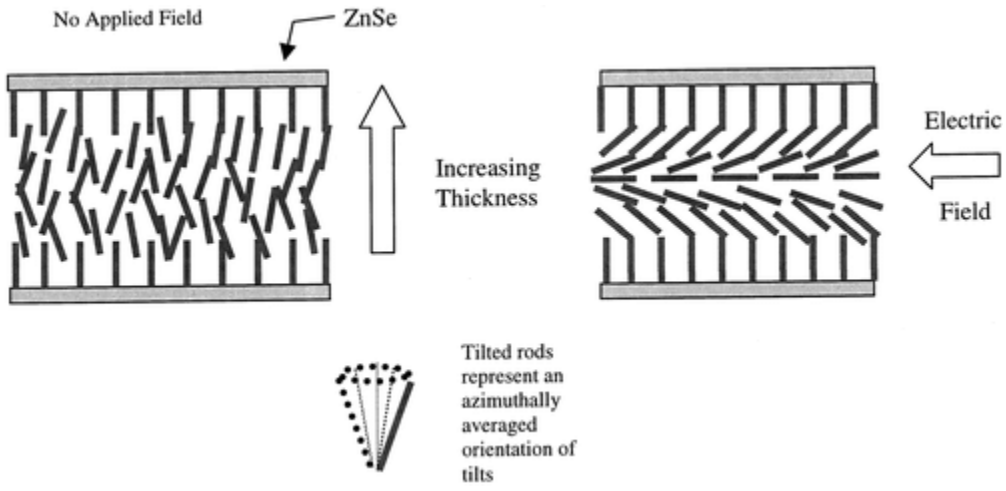

Figure 7 Schematic model of the initial and the transition to the electric field-induced orientation of 5CB within a single nanocavity. The orientations shown are not a quantitative depiction of the canted organization of the 5CB molecules present in the absence of an applied electric field. It is not known if the tilt anisotropy extends completely to the cell wall. The tilt anisotropy noted reflects an average measured over the dimensions of the cell probed by the beam.

We also performed experiments similar to those described for the ultrathin film on a 300 nm thick layer of 5CB. To make these latter measurements, a new ZnSe-supported IDA with identical spacing and pitch was microfabricated using a gold electrode height of 300 nm.

This thick-film sample showed a similar (but less pronounced) tilt alignment than was described above for the ultrathin film cell. Notable changes are attendant with the increase in the cell size as is clearly illustrated by the data presented in Figures 5b and 6b. Most notably, the application of the electric field in this case leads to measurable changes in the difference band intensities measured for both perpendicular and parallel polarizations of the incident light. As expected, the induced orientation of the 5CB is along the direction of the applied field. However, the response of this thicker layer

suggests that some (but not all) of the intensity gained in the $I_{\perp}$ spectra comes from a reorientation of transition moments that have a significant projection along the $I_{\parallel}$ direction. It is interesting to note that the loss of intensity measured for the ν_{CN} mode along the $I_{\parallel}$ direction is less than the gain seen in the $I_{\perp}$ direction (Figure 6b). This indicates that the reorientation of the 5CB molecules in the electric field must also deplete a system of molecular projections that lie along the other remaining (i.e., transverse) cell axis.

When taken together, the data shown in Figures 5 and 6 strongly suggest that interface binding effects are weighted very heavily in the phase properties of 5CB in the 40 nm film. These surface-controlled behaviors make less significant contributions to the overall properties of the sample when the cell dimensions are increased. As we demonstrate below, even more striking effects are evidenced in the field-response dynamics.

Time-Resolved Studies. Step-scan FTIR was used to study the dynamics of the molecular organizations induced by an applied electric field. Unlike conventional FTIR spectroscopy, which uses a single modulation frequency, the mirror in a step-scan interferometer is stepped using a more complex set of modulation frequencies.[29] In descriptive terms, the data are sampled at each retardation and correlated along a second time axis. For kinetic studies using step-scan FTIR, it is necessary that a reproducible sample perturbation be triggered at each retardation. The resultant effects of the perturbation are evidenced in the signal and collected as binned data. Each measurement is repeated for the full range of mirror retardations yielding a two-dimensional array of data composed of one point at each mirror retardation and at each time. After the full set of data is collected, an interferogram can be constructed for any time during the perturbation process. Upon Fourier transform, the extracted interferograms yield time-resolved spectra that show the changes in the sample as it responds to the external perturbation. This qualitative (though technically incomplete)[33] description illustrates the essential elements of the measurement, namely, that the use of a step-scan acquisition effectively decouples spectral multiplexing from the time domain of the sample perturbation. Excellent reviews are available which more thoroughly detail this powerful spectroscopic technique.[28,30]

We first consider time domain data collected on the 40 nm film of liquid crystal. A representative example of a full three-dimensional, time-resolved data set is shown in Figure 8. This measurement (obtained for a 12.6 V square wave pulse 50 ms in duration) was taken with perpendicularly polarized light and is referenced to a constant 0 V background acquired using the same instrumental parameters. After a settling time of 25 ms, the voltage is applied and an immediate response is measured in the orientation of the liquid crystal. By 50 ms, the orientational motions of the 5CB have nearly saturated and the difference peaks plateau. After the applied potential is removed, the sample relaxes completely to its initial 0 V configuration.

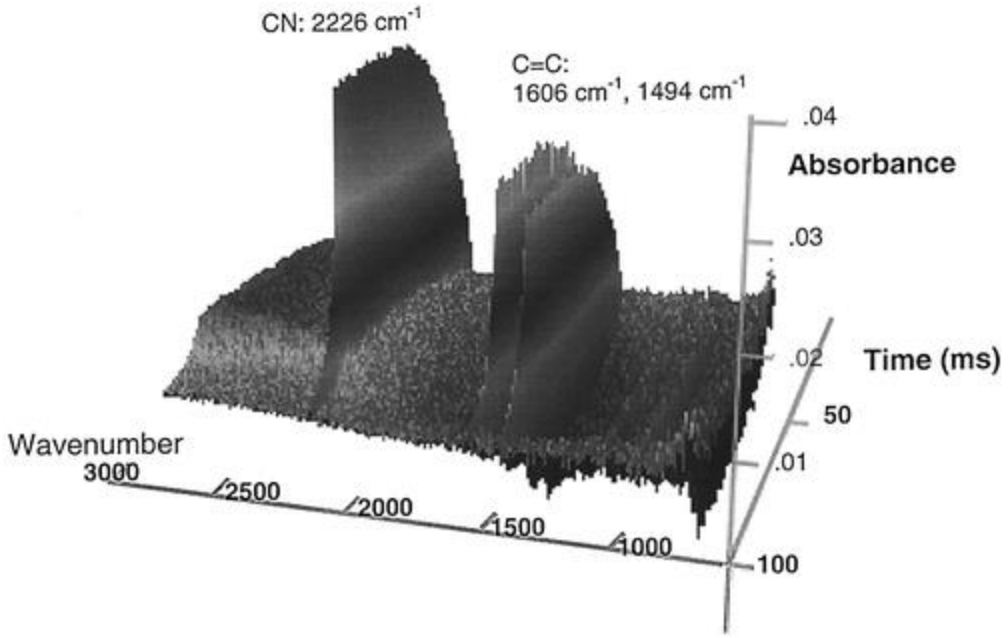

Figure 8 Three-dimensional time-resolved spectrum of 5CB. Prominent modes increase with time after the applied pulse of 12.6 V, plateau when maximum orientation in the applied field is achieved, and then relax back to the preperturbed orientation.

The change in intensity for any given peak, and thus the change in liquid crystal orientation as deduced from its known transition moment direction relative to molecular coordinates, can be seen by extracting component bands from the spectra at incremented times after the applied pulse. An example of such a data set is shown in Figure 9a for the difference band obtained for the ν_{CN} mode. The absorbance of any peak as a function of time during the entire perturbation can also be extracted from the step-scan data set. A plot of three prominent absorption peaks (which increase and then saturate during the application of the pulse) is presented in Figure 9b. These plots mirror the changes in the anisotropy of the 5CB organization with time and contain much information about its complex dynamic response. All the same it is useful to consider a simple (and thus only approximate) model for determining rate constants for the field-induced orientation and subsequent relaxation of the liquid crystal. The simplest functional form for a kinetic fit of the orientation process is a rising exponential given by $A_{on} = C_0(1 - \exp[-kt]) + C_1$ (1) Figure 10a shows a representative fit for the ν_{CN} mode centered at 2226 cm^{-1}. Similarly, the relaxation follows an exponential decay as given by $A_{off} = C_0 \exp[-kt] + C_1$ (2) Figure 10b shows a calculated fit based on this model for the ν_{CN} mode centered at 2226 cm^{-1}. The rate constants of orientation ($k_{orientation}$) and relaxation ($k_{relaxation}$) for four prominent but representative bands (which also have minimal interference from neighboring modes) were calculated using these assumptions to model the 40 nm thin-film data. The calculated rate constants, which show good agreement, are reported in Table 2 and plotted in Figure 11. The data shown are derived from an analysis of the difference bands assigned to the aromatic in-plane C−C stretches (1494, 1606 cm^{-1}), the methyl symmetric C−H stretch (2870 cm^{-1}), and the C:N stretch (2226 cm^{-1}).

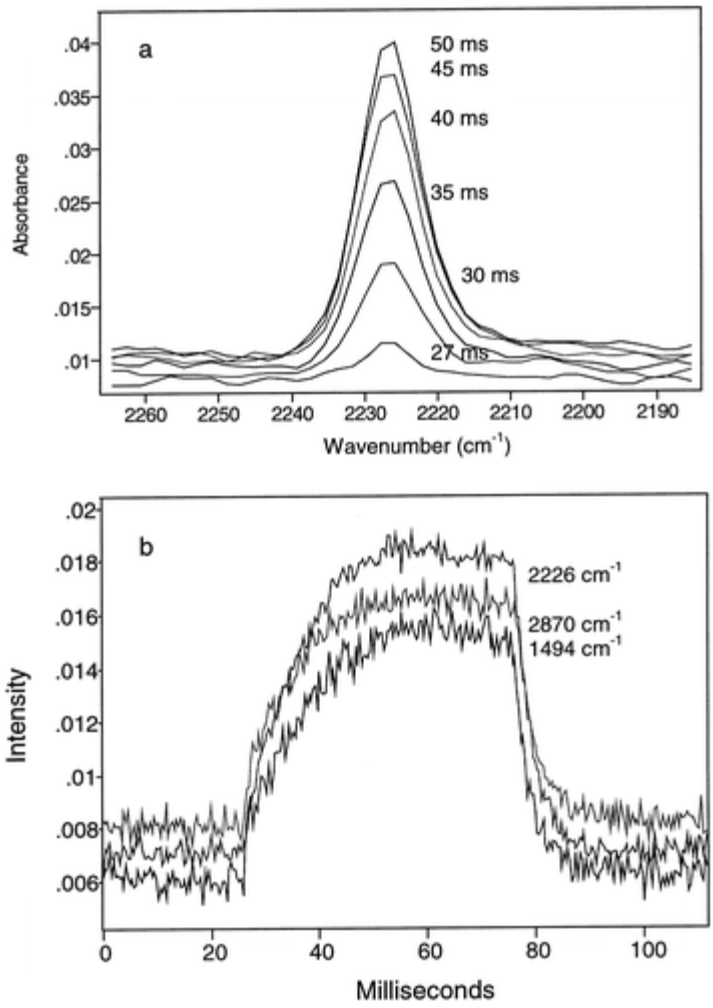

Figure 9 (a) Difference peaks for 2226 cm^{-1} at various times after a 12.6 mV pulse is applied. This cross section of Figure 7 illustrates the time scale for the orientation of 5CB in the electrooptical cell. (b) Intensity traces for representative vibrational mode difference peaks of 5CB upon application and removal of an electric field across the 40 nm thin film. These traces can be fit with rising and decaying exponential functions to determine the rate constants for the orientation and relaxation of 5CB.

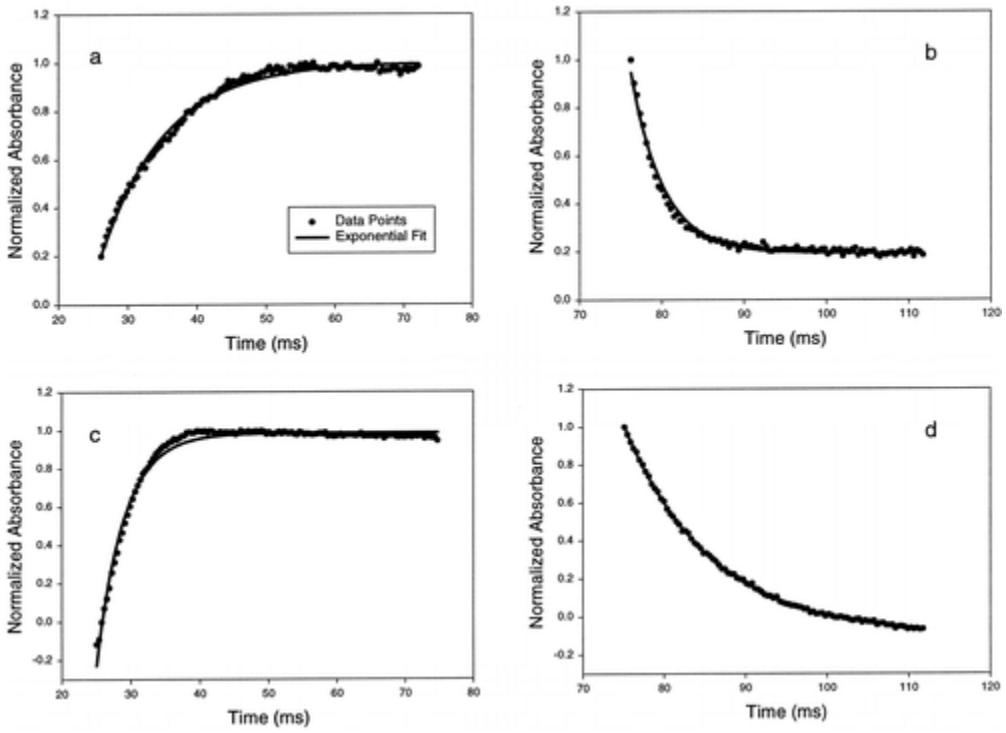

Figure 10 Fits of normalized intensity traces of the 2226 cm^{-1} vibrational mode to exponential functions: (a) and (b) 40 nm cell; (c) and (d) 300 nm cell.

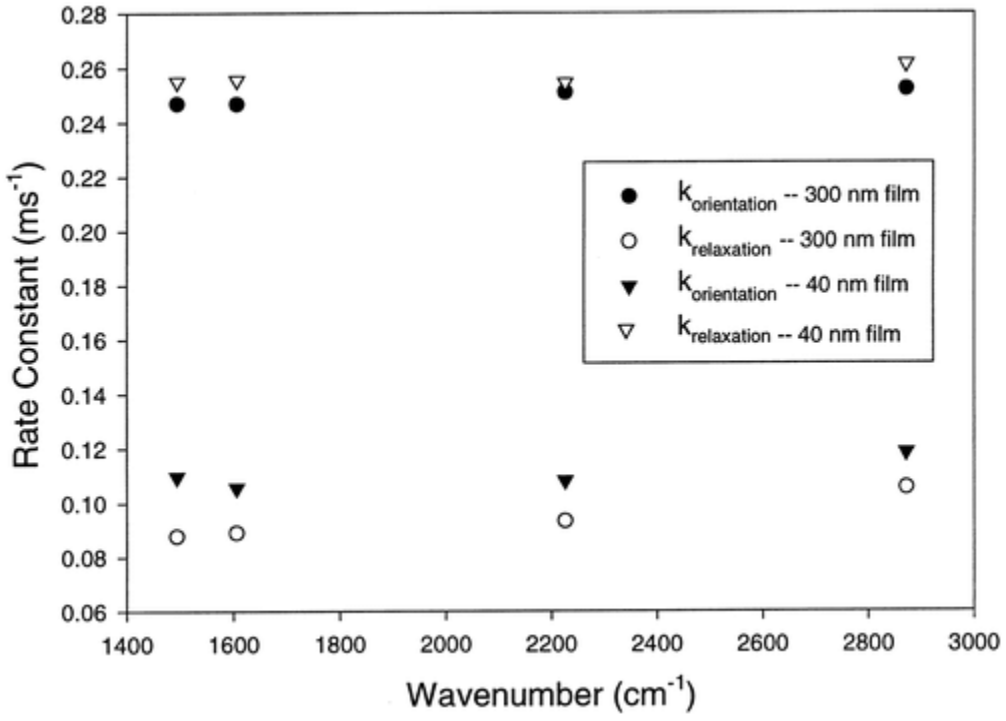

Figure 11 Rate constants for the orientation and relaxation of 5CB under an applied electric field determined from the fits shown in Figure 10. The rate constants for the 40

nm film are represented by triangles showing a larger *k* for relaxation and a smaller *k* for orientation. The rate constants for the 300 nm film are represented by circles and the relationship between rate constants is reversed from that of the 40 nm film with *k* for orientation being larger than *k* for relaxation.

Table 2. Rate Constants Measured for 40 nm Film of 5CB

wavenumber (cm^{-1})	$k_{orientation}$ (ms^{-1})	$k_{relaxation}$ (ms^{-1})
1494	0.110 ± 0.003	0.2551 ± 0.0002
1606	0.106 ± 0.002	0.2556 ± 0.0002
2226	0.108 ± 0.002	0.2545 ± 0.0001
2870	0.118 ± 0.004	0.2613 ± 0.0003

The resolution of the step-scan measurement is sufficient to enable a more detailed examination of the field-induced orientation and subsequent relaxation dynamics. This analysis starts with an appreciation of the fact that the line shapes of vibrational bands in condensed-phase media are frequently determined by the contributions made by inhomogeneous broadening mechanisms. In a nematic liquid crystal, which can exhibit a complex domain structure (and for the thin-film sample examined here, potential perturbations may also arise due to the heavily weighted contributions of molecules experiencing boundary layer interactions), the field-induced responses need not be homogeneous. Rather, the response could reflect the nature of the distribution of structural environments present in the sample. We tested for this sensitivity by sampling the time domain response of the ν_{CN} mode across its heterogeneously broadened line width. The CN stretching mode is well resolved from other bands and an evaluation of the temporal evolution of its (difference) line shape is therefore reasonably straightforward. Rate constants were calculated at the peak maximum, 2226 cm^{-1}, and over the width of the absorption band by taking time slices through both its high- and low-frequency sides (at 2232 and 2220 cm^{-1}, respectively). The resulting rate constants for orientation and relaxation were calculated from fits done as described above; these results are presented in Figure 12a. Clearly, for the 40 nm film, the rate constants calculated for both orientation and relaxation are consistent wherever they are measured across the line width of the peak. It is significant to note that, for this sample, the orientation process is markedly slower than that for relaxation.

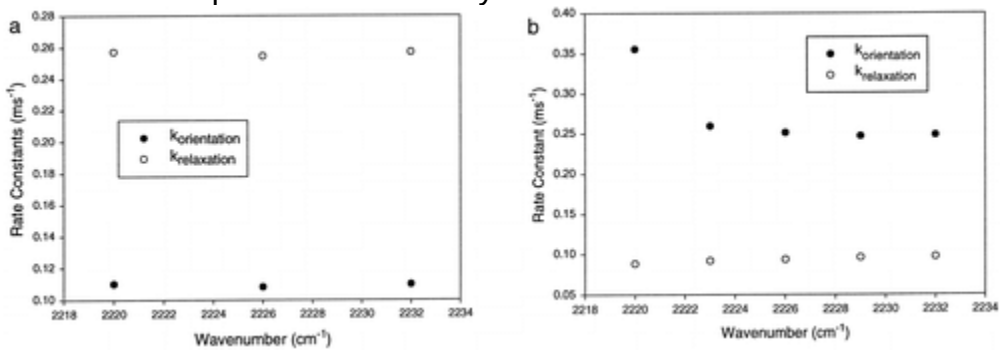

Figure 12 Rate constants measured across the width of the 2226 cm^{-1} vibrational mode: (a) 40 and (b) 300 nm film. Kinetic inhomogeneity is seen in the orientation of the 5CB in the 300 nm film while the other processes appear to be kinetically homogeneous.

We also examined the dynamics evidenced in a thicker cell (300 nm) with the step-scan FTIR method using the same methods applied to the 40 nm film. Two representative fits for determination of the rate constants (calculated at the 2226 cm^{-1} maximum of the ν_{CN} mode) are shown in Figure 10c and d. The rate constants calculated for the orientation and relaxation of 5CB as deduced from several prominent peaks are shown in Figure 11 and summarized in Table 4. The rate constants are again found to be internally self-consistent for different vibrational modes of the molecule but they are clearly different from the rate constants measured for the ultrathin film. The rate constant for orientation is much larger in the 300 nm film (by a factor of ~2.25), indicating that its field-induced motion occurs much more rapidly than for the ultrathin film. The relaxation process has a smaller rate constant, however, indicating that it takes longer for the molecules to return to the lower energy condition of the net anisotropy found in the initial state after the field is removed. As we describe below, these results are consistent with the hypothesis that the properties of the ultrathin surface film are strongly impacted by the surface interactions that attend the nanoscale confinement.

Table 3. Rate Constants off Peak Maximum of CN Stretch, 400 Å Thin Film

wavenumber (cm^{-1})	$k_{orientation}$ (ms^{-1})	$k_{relaxation}$ (ms^{-1})
2220	0.110 ± 0.003	0.2572 ± 0.0002
2226	0.108 ± 0.002	0.2545 ± 0.0001
2232	0.110 ± 0.003	0.2569 ± 0.0002

Table 4. Rate Constants Measured for the 3000 Å Film of 5CB

wavenumber (cm^{-1})	$k_{orientation}$ (ms^{-1})	$k_{relaxation}$ (ms^{-1})
1494	0.247 ± 0.004	0.0877 ± 0.0007
1606	0.247 ± 0.004	0.0890 ± 0.0005
2226	0.251 ± 0.005	0.0933 ± 0.0006
2872	0.253 ± 0.011	0.106 ± 0.004

We again sampled time slices across the line width of the ν_{CN} mode to test for the presence of kinetic inhomogeneity. Rate constants were measured at 2220, 2223, 2226, 2229, and 2232 cm^{-1}. These results are summarized in Table 5 and plotted in Figure 12b. It is most striking that the rate constants measured for the field-induced orientation of the thicker film are no longer kinetically homogeneous across the line width of the ν_{CN} peak. This rate dispersion does not appear strongly, however, in the rate constants calculated for the decay of the oriented state (i.e., the relaxation processes behave in a kinetically homogeneous way). The data thus suggest the presence of a nonhomogeneous thin-film structure in this sample.

Table 5. Rate Constants off Peak Maximum of CN Stretch, 3000 Å Thin Film

wavenumber (cm^{-1})	$k_{orientation}$ (ms^{-1})	$k_{relaxation}$ (ms^{-1})
2220	0.353 ± 0.008	0.088 ± 0.002
2223	0.259 ± 0.005	0.0918 ± 0.0007
2226	0.251 ± 0.005	0.0933 ± 0.0006
2229	0.247 ± 0.005	0.0959 ± 0.0008
2232	0.248 ± 0.005	0.097 ± 0.001

Discussion

Taken together, the data presented above demonstrate that the dynamics of 5CB under an applied electric field differs significantly between an ultrathin film and one with a larger bulk component. The data strongly suggest that the 40 nm film exhibits a complex, anisotropic change in its net alignment in response to the applied field. This feature, perhaps more than any other, makes it clear that the interactions with the ZnSe surface strongly affects the orientations adopted by and the relaxation processes of the 5CB molecules throughout the sample. We had initially believed that the 5CB molecules would align preferentially along the direction defined by the gold electrodes with the orientation of its long axis lying along the plane of the ZnSe crystal. The polarization studies clearly suggest that the 5CB orientation (absent the applied field) is actually strongly anchored to give a significant projection along the surface normal direction. This orientation is a thermodynamically directed state since, even after repeated polarization cycles, the system completely relaxes to this configuration. The 5CB molecule is ~16 Å long. The cavity defined by the 40 nm Au bands is therefore on the order 25 times the contour length defined by this molecular dimension. The anchoring effect of the ZnSe surface is therefore seen to be both robust and reasonably long-ranged. We know from X-ray photoelectron spectroscopy (XPS) data (not shown) that the ZnSe surface is heavily oxidized: a complex mixture of oxides and carbonates seems to terminate this surface even after careful cleaning procedures. In this light then, the strong anchoring we see and the overall anisotropy of the orientation induced, is perhaps not that surprising after all.

The static polarization experiments further serve to reveal the differences that exist between the organization and field-induced responses of the 5CB films in 40 and 300 nm thick cells. For example, the intensity of the CN difference band, the transition moment of which has a significant projection along the long axis of the molecule, grows markedly in intensity for both cells upon application of the electric field when interrogated with perpendicularly polarized light. In the thinner film, there are no corresponding intensity changes seen for scans taken with light polarized parallel to the IDA fingers (a very surprising result given the azimuthally averaged tilt alignment described above). For the thicker film, however, intensity changes (negative) are seen in the parallel polarization spectra; these intensity changes, while significant, are insufficient to account for the increases seen in the perpendicular polarization data. Taken at face value, the data suggest that the 5CB molecules still retain a net

anisotropy, one demonstrating a preferred (though weaker) projection on the surface normal direction in the thicker film.

It is important to note at this point that some degree of caution is warranted in interpreting the intensity changes seen in the static polarization data presented in Figure 5. These are difference spectra and only report on changes in the net anisotropy of the 5CB organization in response to an applied electric field. A complex initial alignment in the sample, such as that which gives rise to the data shown in Figure 5, will give a difference spectrum that masks important contributions to the net organization of the sample. For example, any initial dipole moment projections lying along the perpendicular polarization direction will go undetected in the field response data measured in that direction. If we assume that the population of molecules oriented along the parallel direction is similar to that lying along the perpendicular direction (a reasonable assumption given the large 15 μm spacing of the electrodes and the likely stronger anisotropy that would arise from the ZnSe crystals ─ which is in fact supported by experimental data), then the difference spectra shown in Figure 5 are insensitive to at least 30% of the net contents of the sample. By extension, the alignment inferred from the data shown in Figure 5a cannot be characterized with regard to any net projections of the 5CB along the perpendicular direction. Rather, we can say that any field-induced tilt off the cell normal direction must be highly aligned along this one vector.

It is important to point out that it is likely that the gold electrode bands do induce a net anisotropy in the 5CB samples. We found that shearing the sample along the direction of the gold bands does not induce any stable ordering (that is, order that recovers after repeated cycling through potential perturbations) of the 5CB director. The boundary interactions at the gold, however, could induce anisotropies in the organization of the 5CB.[12] We are currently examining the relative importance of these latter interactions via the construction of electrode arrays with very different pitches. There are numerous issues of interest in these latter experiments, not the least of which is the fact that the limiting dimensions of some of these systems will exceed the diffraction limits of the mid-infrared experiments used here. This fact presents both challenges and opportunities for experimental design that we will explore in future publications.

We turn finally to a consideration of the time domain spectroscopy and the nature of dimensional scaling seen in the electrooptical dynamics of the liquid crystalline material. The data shown in Figure 11 are particularly striking in several regards. Perhaps of greatest interest is the inversion seen in the relative ranking of the orientation and relaxation rate constants measured for the two limiting cell dimensions. The electric field-induced orientation of 5CB in the 40 nm thick sample is much slower than is the corresponding process in the thicker cell (the rate constant for the 300 nm film is ~2.25 times faster than the orientational rate constant for the 40 nm film). Perhaps more intriguing, the relative relaxation rates in these two cells show an inverted ranking; the field-induced orientation decays much faster in the thin cell (~2.73 times faster) than is found in the thicker sample. There are several ways one might rationalize this behavior. First, we discount any perturbations that result from confinement effects on the apparent viscosity of the medium. As an intrinsically anisotropic medium, 5CB cannot change its director orientation in a nanoscale cavity without a coupled center of mass motion of the molecules (to avoid massive effective pressure changes at the cell walls). These

motions can be frustrated by walls and is analogous to the functioning of lubricants.[34] The slow orientation of 5CB in the thin-cell sample cannot be due to an effect of this sort, since, as we see, its relaxation rate is not similarly perturbed, but, rather, is comparatively fast (approaching that found for field-induced motions in more bulklike samples). We believe the origin of this effect lies in the surface anchoring interactions occurring with the ZnSe crystal surfaces. These interactions strongly pin the orientations of the 5CB molecules and thus appear to serve as a force that the field-induced motions must overcome. Similarly, this interaction serves to drive the decay of the field-aligned state. These latter effects are not as pronounced in the more bulklike sample. The interactions do not organize collectively throughout the sample, and as a result, the application of the electric field leads to a more facile motion of 5CB molecules. The fact that the decay of this latter state is reasonably slow suggests that the process is not strongly driven. We believe it is consistent with a thermal redistribution toward a more random state. We should point out here, however, that these descriptions provide a simple rationalization which accounts for trends developed in simple single-exponential fits of the data. There likely exist more subtle features in the dynamics which these experiments do not test. We plan to more sensitively test for deviations from single-exponential responses in future work.

Another interesting dimensional scaling of the orientational dynamics is seen in the data presented in Figure 12. In the nanoscale cavity, the 5CB molecules appear to respond as a “coherent” ensemble in that the rate constants measured across the line width of the ν_{CN} band are kinetically homogeneous. In the thicker cell, considerable kinetic heterogeneity is found in the orientation rate constants measured across the inhomogeneously broadened ν_{CN} line width. This response suggests that this film may be characterized by a complex polydomain structure. This structure has not been independently established using other methods.[35] Still, it seems to be the easiest way to rationalize the presence of molecules in this cell with ν_{CN} band maximums that are shifted by several wavenumbers and exhibit orientation rate constants that differ by more than a factor of 2. We should point out that the literature contains many reports of kinetic heterogeneity in the electrooptical responses of bulklike liquid crystal films.[6,7,9,10,22,36] A few of the reports have attributed these effects to an intrinsic heterogeneous response of the different segments of the 5CB structure (e.g., the rigid core and the flexible tail). We do not believe that segmental arguments of this type are valid in this context. First, the rate behaviors of concern here have millisecond lifetimes. Millisecond rate behaviors are on a time scale that is far too slow to distinguish the segmental dynamics of 5CB (which should occur on a picosecond time scale). The current results demonstrate a strong sample (i.e., size)-dependent scaling of the rate dispersion measured via a single vibrational mode (the ν_{CN} mode), a feature we intuitively associate with a polydomain structure in the thicker sample. It is interesting to note that a corresponding rate heterogeneity is not seen in the relaxation of the thicker 5CB sample. Again, we believe that this is consistent with a weakly driven thermal decay toward a less anisotropic state.

This study demonstrates an interesting approach to examining the dynamics of thin organic media through the coupled use of time domain vibrational correlation spectroscopy and methods of microfabrication. In this report, we did not attempt to alter any aspect of the interactions occurring between the cell wall and the 5CB other than

through changes in the gold electrode thickness. As noted earlier, we will shortly describe more complicated fabrication schemes that enable us to explore the effects of narrower gold band spacings, studies that will more strongly weight contributions made by molecules residing adjacent to the metal surfaces. In principle, these interactions can be sensitively engineered via the use of self-assembled monolayers (SAMs) as has been so elegantly demonstrated by Abbott and co-workers.[11,15] As we will show, it appears very likely that SAMs can also be used to modify the interactions occurring at the surface of ZnSe crystals and thus every aspect of the wall anchoring interactions should be available for molecular design and direct study. We will describe our progress along these lines of study in future publications.

Acknowledgment

We gratefully thank the National Science Foundation for their support of this work (Grant CHE 9626871) and the Defense Advanced Research Projects Agency for providing the funds used to purchase the step-scan spectrometer.

This article references 36 other publications.

1. **1**

   Tallman, D. E.; Pae, Y.; Bierwagen, G. P. *Corrosion***1999**, *55*, 779−786.

2. **2**

   TeGrotenhuis, W. E.; Cameron, R. J.; Butcher, M. G.; Martin, P. M.; Wegeng, R. S. *Sep. Sci. Technol.***1999**, *34*, 951−974.

3. **3**

   Guo, Y.; Colon, L. A. *Anal. Chem.***1995**, *67*, 2511−2516.

4. **4**

   Stuart, D. I.; Jones, Y. E. *Curr. Opin. Struct. Biol.***1995**, *5*, 735−743.

5. **5**

   Goodman, L. A. *Introduction to Liquid Crystals*; Plenum: New York, 1995.

6. **6**

   Kaito, A.; Wang, Y. K.; Hsu, S. L. *Anal. Chim. Acta***1986**, *189*, 27−40.

7. **7**

Shilov, S. V.; Okretic, S.; Siesler, H. W. *Vib. Spectrosc.***1995**, *9*, 57−63.

8. **8**

   Ekgasit, S.; Fulleborn, M.; Siesler, H. W. *Vib. Spectrosc.***1999**, *19*, 85−91.

9. **9**

   Gregoriou, V. G.; Chao, J. L.; Toriumi, H.; Palmer, R. A. *Chem. Phys. Lett.***1991**, *179*, 491−496.

10. Nakano, T.; Yokoyama, T.; Toriumi, H. *Appl. Spectrosc.***1993**, *47*, 1354−1366.
11. **11**

    Drawhorn, R. A.; Abbott, N. L. *J. Phys. Chem.***1995**, *99*, 16511−16515.

12. **12**

    Abbott, N. L. *Curr. Opin. Colloid Interface Sci.***1997**, *2*, 76−82.

13. **13**

    Gupta, V. K.; Abbott, N. L. *Langmuir***1996**, *12*, 2587−2593.

14. **14**

    Gupta, V. K.; Miller, W. J.; Pike, C. L.; Abbott, N. L. *Chem. Mater.***1996**, *8*, 1366−1369.

15. **15**

    Gupta, V. K.; Abbott, N. L. *Science***1997**, *276*, 1533−1536.

16. **16**

    Miller, W. J.; Abbott, N. L. *Appl. Phys. Lett.***1996**, *69*, 1852−1854.

17. **17**

    Blanchard, R. M.; Luginbuhl, A. R.; Nuzzo, R. G. *Anal. Chem.***2000**, *72*, 1365−1372.

18. **18**

    Gray, G. W.; Harrison, K. J.; Nash, J. A. *Electron. Lett.***1973**, *9*, 130−131.

19. **19**

Freedericksz, V.; Repiewa, A. Z. *Phys.***1927**, *42*, 352.

20. Ashford, A.; Constant, J.; Kirton, J.; Raynes, E. P. *Electron. Lett.***1973**, *9*, 118−120.
21. **21**

Toriumi, H.; Sugisawa, H.; Watanabe, H. *J. Appl. Phys.***1988**, *27*, L935−L937.

22. **22**

Urano, T. I.; Hamaguchi, H. *Chem. Phys. Lett.***1992**, *195*, 287−292.

23. **23**

Soref, R. A. *J. Appl. Phys.***1974**, *45*, 5466−5468.

24. **24**

Oh-e, M.; Kondo, K. *Appl. Phys. Lett.***1995**, *67*, 3895−3897.

25. **25**

Chidsey, C. E. D.; Feldman, B. J.; Lundgren, C.; Murray, R. W. *Anal. Chem.***1986**, *58*, 601−607.

26. **26**

Niwa, O. *Electroanalysis***1995**, *7*, 606−613.

27. **27**

Transition moments projecting on the parallel direction will have zero intensity near the Au electrode due to the operation of the dipole surface-selection rule. See: Parikh, A. N.; Allara, D. L. *J. Chem. Phys.***1992**, *96*, 927. *Vibrational Spectroscopy of Molecules on Surfaces Methods of Surface Characterization*; Yates, J. T., Madey, T. E., Eds.; Plenum: New York, 1987; Vol. 1. Projection of these same moments on the perpendicular direction will be enhanced for similar reasons. The 15 μm spacing used here, however, is large compared to the distances impacted by these perturbations. In principle, the optical effects occurring in the boundary layer of a cell such as this provide a potentially sensitive means to probe adsorbate electrode dynamics. In the context of the present study, they serve merely as a scalar weighting the intensities in the parallel and perpendicular director regions.

28. **28**

Manning, C. J.; Palmer, R. A.; Chao, J. *Rev. Sci. Instrum.***1991**, *62*, 1219−1229.

29. **29**

Crocombe, R. A.; Compton, S. V. *The Design, Perfomance and Applications of a Dynamically-Aligned Step-Scan Interferometer*, Bio-Rad Digilab Division, 1991.

30. Palmer, R. A.; Manning, C. J.; Pzepiela, J. A.; Widder, J. M.; Chao, J. L. *Appl. Spectrosc.***1989**, *43*, 193−195.

31. **31**

Hatla, A. *Mol. Cryst. Liq. Cryst.***1984**, *74*, 195−207.

32. **32**

Sakamoto, K.; Naoki, I.; Arafune, R.; Ushioda, S. *Vib. Spectrosc.***1999**, *19*, 61−69.

33. **33**

The Bio-Rad 896 interferometer uses a second modulation for servocontrol and thus a more complex computational algorithm is used. See: reference 28.

34. **34**

Granick, S. *Phys. Today***1999**, *52*, 26−31.

35. **35**

Domains in the nematic phase of this material in bulk can range to length scales of the order of the size of the electrode spacing used in these experiments. We have not determined the nature of the domains present in our arrays (if any) using optical microscopy because the microstructure of the ZnSe crystal precludes this type of examination of the assembled cell.

36.

Urano, T. I.; Hamaguchi, H.-O. *Appl. Spectrosc.***1993**, *47*, 2108−2113.